Aalborg Universitet

AALBORG UNIVERSITY

DENMARK

Sensor Fusion and Model Verification for a Mobile Robot

Bisgaard, Morten; Vinther, Dennis; Østergaard, Kasper Zinck; Bendtsen, Jan Dimon; Izadi-Zamanabadi, Roozbeh

Link to publication from Aalborg University

SENSOR FUSION AND MODEL VERIFICATION FOR A MOBILE ROBOT

Morten Bisgaard, Dennis Vinther, Kasper Østergaard,
Jan Bendtsen and Roozbeh Izadi-Zamanabadi
Department of Control Engineering, Aalborg University
Fredrik Bajersvej 7C
DK-9220 Aalborg East, Denmark.
Email: {mbis00,drvi00,kzoe00,dimon,riz}@control.aau.dk

Abstract

This paper presents the results of modeling, sensor fusion
and model verification for a four-wheel driven, four-wheel
steered mobile robot moving in outdoor terrain. The model
derived for the robot describes the actuator and wheel dy-
namics and the vehicle kinematics, and includes friction
terms as well as slip. An Unscented Kalman Filter (UKF)
based on the dynamic model is used for sensor fusion, feed-
ing sensor measurements back to the robot controller in an
intelligent manner. Through practical experiments with the
robot, the UKF is demonstrated to improve the reliability
of the sensor signals significantly, and the model is seen to
show surprisingly good agreement with the practical exper-
iments.

Keywords

Autonomous Robots, Newtonian Mechanics, Unscented
Kalman Filtering

1   Introduction

This paper reports part of the work carried out in connec-
tion with a recent project[1] concerning the construction of a
robot for autonomous surveying of agricultural fields. The
robot has to navigate to certain waypoints (measurement
locations), where digital images of the crops, weeds, etc.
can be acquired. Image analysis may then be used in or-
der to obtain estimates of the crop and weed density at
each measurement location. This information will be com-
bined for each location to yield a digitized weed map of
the field, opening up opportunities for the farmer to adjust
the application of fertilizer and pesticides according to the
state of the field (so-called *precision farming*). The robot
is equipped with GPS and various onboard sensors, which
will not only help in the exact determination of the location
where each image is taken, but also provide measurements
for an estimation of the robot's position and orientation for
use in tracking control algorithms.

The robot is equipped with independent steering and
drive motors (8 DC motors in total). The motors are con-

trolled by individual controllers implemented in four mi-
crocontrollers, one for each wheel, which are connected
to a main computer via a CAN-bus. Rotation speed or
torque references can thus be set individually for each mo-
tor from the main onboard computer, a PC104 with a 133
MHz AMD5x86 CPU and 32 MB RAM running Linux.
The robot is furthermore equipped with various sensors; a
row camera is used for navigating relative to crop rows, a
doppler radar is used to measure ground speed, and a com-
pass is mounted to obtain the orientation of the robot. The
robot is also equipped with a gyro to measure yaw accel-
erations. An antenna is mounted for communication via a
WLAN interface connecting the robot to a centrally posi-
tioned computer, which handles generation of the overall
path plan for the system, storing image data etc.

Figure 1. The API II robot. The dimensions of the robot
are $150cm$ (length) by $100cm$ (width) by $107cm$ (height).
It weighs $226.5kg$.

In the literature on modeling and control of wheeled
mobile robots, the equations of motion are typically de-
rived using the Lagrangian approach [1, 2] or Newton-
Euler methods [6, 8] . It is typically assumed in such
modeling approaches that there is neither slip nor skidding,
since the model is often used directly for control design.
This assumption is not likely to be satisfied in outdoor en-
vironments, however. In this paper, we present a dynamic
model of the robot that describes the dynamics from input
torques on the wheels to resulting translational and rota-
tional velocities of the robot body. The model takes the

---

actuator and wheel dynamics and the vehicle kinematics into account, and includes friction terms as well as slip. By calculating the equations of motion in a fixed non-inertial frame, we avoid having to convert velocities and positions between moving coordinate frames. We also present a validation of the model against actual test data.

The purpose of this first-principles model is to apply it in an Unscented Kalman Filter (UKF), which can be used for sensor fusion, feeding sensor measurements back to the robot controller in an intelligent manner. This gives various benefits, such as improved accuracy and, in some cases, increased bandwidth of the sensor measurements. A further aim of the modeling and sensor fusion work presented here is to be able to use it in fault detection and fault tolerant control, but these issues will be dealt with in a later publication.

2 Mechanical Model

In the following, the mechanical model of the robot is presented.

2.1 Model Framework

The position and orientation of the robot is described by a posture vector $\bar{\chi} = [\bar{x}, \bar{y}, \bar{\theta}]^T \in \mathbb{R}^2 \times \mathbb{S}$, which is defined in an inertial reference frame $\mathcal{N}$; coordinates defined in this frame will be denoted by $\bar{(\cdot)}$. Given that the robot will be moving in outdoors terrain, it is also necessary to take into account the non-even terrain. This will be done by introducing a non-inertial reference frame $\mathcal{M}$, in which we will derive the model as if the robot is moving in a plane. When the robot is moving in uneven terrain (given by a roll angle $\psi_x \in \mathbb{S}$ and a pitch angle $\psi_y \in \mathbb{S}$), its trajectory can be found by rotating $\mathcal{M}$ relative to $\mathcal{N}$ before integrating the accelerations found in $\mathcal{M}$. The equations of motion are developed in this frame; coordinates defined in $\mathcal{M}$ will therefore be unadorned. Mapping from $\mathcal{N}$ to $\mathcal{M}$ is performed by multiplying by the rotation matrix

$R_{\bar{\psi}} =$

$$\begin{bmatrix} \cos \bar{\psi}_x & 0 & \sin \bar{\psi}_x \\ -\sin \bar{\psi}_x \cos \bar{\psi}_x \sin \bar{\psi}_y & \cos(\bar{\psi}_y) & (\cos \bar{\psi}_x)^2 \sin \bar{\psi}_y \\ -\sin \bar{\psi}_x \cos \bar{\psi}_y & -\cos \bar{\psi}_x \sin \bar{\psi}_y & \cos \bar{\psi}_x \cos \bar{\psi}_y \end{bmatrix}$$

Another (non-inertial) reference frame $\mathcal{B}$ is fixed below the center of mass (CoM) of the robot at ground level. This reference frame is aligned with the robot, with the x-axis pointing in the forward direction of the robot; coordinates defined in this frame will be denoted by $\tilde{(\cdot)}$, i.e., $\chi = [\tilde{x} \ \tilde{y} \ \tilde{\theta}]^T \in \mathbb{R}^2 \times \mathbb{S}$ is the posture vector in the $\mathcal{B}$ frame. Mapping from $\mathcal{M}$ to $\mathcal{B}$ is performed by multiplying by the rotation matrix

$$R_{\tilde{\theta}} = \begin{bmatrix} \cos \theta & \sin \theta & 0 \\ -\sin \theta & \cos \theta & 0 \\ 0 & 0 & 1 \end{bmatrix}$$

The robot and its two primary reference frames are illustrated in Figure 2, where also the posture vector and

the orientation $\beta_i, i = 1, \ldots, 4$ of each wheel is shown. The position of the contact point of each wheel is fixed with respect to the $\mathcal{B}$-frame.
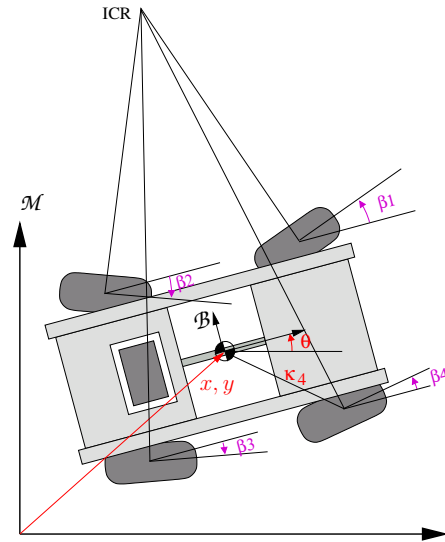

Figure 2. Definitions of the $\mathcal{B}$ and $\mathcal{M}$ frames with the steering angles of the wheels and the posture vector shown in the $\mathcal{M}$ frame. κ_4 indicates the line between the center of the robot and the 4th wheel. The ICR (instantaneous center of rotation) is the point where lines through the contact point of each wheel perpendicular to the instantaneous velocity of the wheel intersect.

The positions of the wheels relative to the center of mass are defined by four vectors of constant length κ_i, which are fixed in the $\mathcal{B}$ frame at corresponding angles $\tilde{\gamma}_i$. The values $\kappa_1 = 0.782m, \kappa_2 = 0.613m, \kappa_3 = 0.646m$ and $\kappa_4 = 0.808m$ were found experimentally along with the corresponding angles $\tilde{\gamma}_1 = 37.8°, \tilde{\gamma}_2 = 128.5°, \tilde{\gamma}_3 = 233.8°$ and $\tilde{\gamma}_4 = 319.9°$ by using four weights to determine the mass distribution of the complete robot.

The dynamic modelling of the robot is inspired by car models used in the automotive industry with [5] as a specific example, where a simple differential braking extension to the standard motor-cycle model with one front and one rear wheel is used. The model sought here is a relatively simple model that captures the particular features of the robot. It is thus chosen to model one wheel at a time, and then construct the model of the vehicle motion based on the forces and torques with which the wheels affect the main body.

2.2 Actuators

Firstly, all four wheels can be placed in steering angles independent of one another and of the ICR (see Figure 2). Secondly, the individual wheels can provide independent propulsion forces to the robot. The actuators are simple DC-motors, so their models are straightforward:

$$\frac{\beta_i}{\beta_{ref,i}} = \frac{K_s K_{m,s}}{(J_{m,s} R_{a,s})s^2 + (b_s R_{a,s} + K_{m,s}^2)s + K_s K_{m,s}} \tag{1}$$

where $\beta_i, i = 1, \ldots, 4$ is the steering angle of wheel i, K_s is a feedback gain, $K_{m,s} = 0.1 Nm/A$, $R_{a,s} = 1.43\Omega$ and $J_{m,s} = 3.1 \times 10^{-4} kgm^2$ are the steering motor gain constant, armature resistance and inertia, respectively. $b_s = 3.0 \times 10^{-3} Nms/rad$ is a friction coefficient and s is the laplace operator.

The propulsion motors are modelled slightly differently, since the mass of the robot $m = 226.5 kg$ has a significant influence on the resulting torque through the back-electromotoric force. That is, the motor inertia is considered negligible compared to the inertia of the robot, which means that the motor dynamics are ignored in the model. The propulsion model for wheel i is found to

$$\tau_i = \frac{K_{m,p}}{R_{a,p}} \tau_{ref,i} - \left(\frac{K_{m,p}^2}{R_{a,p}} + b_p \right) \dot{\phi}_i \qquad (2)$$

where τ_i is the resulting torque of wheel i, $K_{m,p} = 0.31 Nm/A$ and $R_{a,p} = 0.017\Omega$ are the propulsion motor gain constant and armature resistance, respectively. $b_p = 0.37 Nms/rad$ is a friction coefficient. $\dot{\phi}_i$ is the rotation speed of wheel i. All of the parameters were found experimentally.

2.3   Tire Model

The robot motion is generated by the friction between the wheels and the ground. These friction forces are modelled in the following.

In figure 3 a general free-body diagram is shown, from which the dynamic model will be derived. The forces $F_{xi} \in \mathbb{R}^3, i = 1, \ldots, 4$ are the propulsion forces supplied by the actuators, while $v_i = [\dot{x} \ \dot{y} \ 0]^T$ is the actual velocity of wheel i and $\alpha_i \in \mathbb{S}$ is the slip angle of wheel i at any given time. The slip angle is defined as the angle between the actual velocity of the wheel and the orientation of the wheel given by the steering angle.
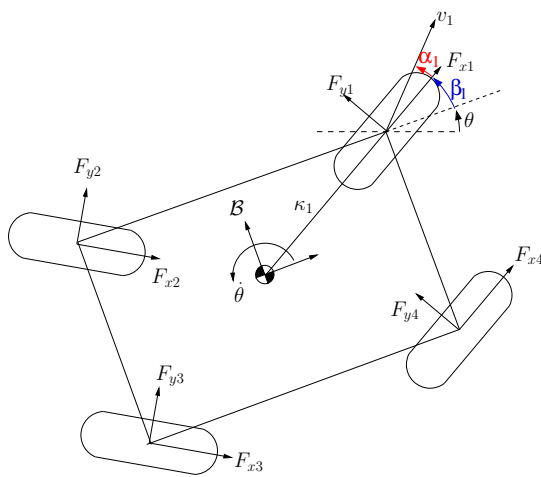

Figure 3. The general setup for the dynamic robot model.

The purpose of the tire model is to describe the sideways friction forces between the tires and the ground, which make the robot capable of turning when the wheels

turn. This friction results in the forces $F_{yi} \in \mathbb{R}^3$ as shown in Figure 3 which depend on the slip angles of the wheels (α_i). In the literature—see e.g., [5]—the friction forces are typically modeled as being directly proportional to the slip angle. This simple model does not take speed-dependent friction phenomena such as viscous friction into account, however, and the following model is therefore used:

$$\|F_{yi}\| = -(c_{f_1} + c_{f_2} \|v\|)\alpha_i \qquad (3)$$

where the positive scalars $c_{f_1} = 40N$ and $c_{f_2} = 4000 Nm/s$ are so-called cornering stiffness coefficients representing stiction and speed-dependent friction phenomena, respectively. $\|v\| = \sqrt{\dot{x}^2 + \dot{y}^2}$ is the translational speed of the robot in the $\mathcal{M}$-frame. The coefficients depend on the composition of the soil on which the robot drives, and were found through numerical fitting to experimental data.

The slip angle $\alpha_i \in [-\frac{\pi}{2}, \frac{\pi}{2}]$ is defined heuristically from F_{xi} to the actual velocity of the wheel v_i in quadrant 1 and 4 and from v_i to F_{xi} in quadrant 2 and 3. v_i is a sum of two contributions, one from the velocity of the CoM v and one from the rotation of the robot around the CoM, which is given as $v_{ti} = \dot{\theta}\kappa_i$ (see below). Since v_{ti} is perpendicular to the line κ_i connecting the CoM and the contact point of wheel i, v_i can be written as follows:

$$v_i = v + v_{ti} = \begin{bmatrix} \dot{x} - \dot{\theta}\tilde{\kappa}_i \sin(\tilde{\gamma}_i + \theta) \\ \dot{y} + \dot{\theta}\tilde{\kappa}_i \cos(\tilde{\gamma}_i + \theta) \\ 0 \end{bmatrix} \qquad (4)$$

Through some slightly tedious geometry, the slip angle can then be calculated as

$$\alpha_i^* = \tan^{-1} \left(\frac{\dot{y} + \dot{\theta}\kappa_i \cos(\tilde{\gamma}_i + \theta)}{\dot{x} - \dot{\theta}\kappa_i \sin(\tilde{\gamma}_i + \theta)} \right) - \beta_i - \theta \quad (5)$$

$$\alpha_i = \begin{cases} \pi - \alpha_i^* & \text{for} \quad \pi/2 \leq \alpha_i^* < 3\pi/2 \\ \alpha_i^* - 2\pi & \text{for} \quad 3\pi/2 \leq \alpha_i^* \\ \alpha_i^* & \text{for} \quad \alpha_i^* < \pi/2 \end{cases} \quad (6)$$

where the manipulations in (6) are performed in order to ensure that $\alpha_i \in [-\frac{\pi}{2}, \frac{\pi}{2}]$.

2.4   Equations of Motion

The translational motion of the robot is governed by the acceleration in the $\mathcal{M}$-frame, $\ddot{\chi} = [\ddot{x} \ \ddot{y} \ \ddot{\theta}]^T$. The force acting on the robot yielding translational motion is given as the sum of the sideways friction forces F_{yi}, the propulsion forces F_{xi} and the centripetal forces which affect the robot. In Figure 3 the sideways friction and propulsion forces are shown; these forces can be projected onto the $\mathcal{M}$-frame in a fairly straightforward manner. The centripetal force is calculated based on the ICR (see Figure 2). Define the rotation vector $\omega = [0 \ 0 \ \dot{\theta}]^T$; the acceleration caused by the centripetal force a_c is given by

$$a_c = \omega \times (\omega \times r) = \omega \times v \qquad (7)$$

where $r \in \mathbb{R}^3$ is the vector from the ICR to the CoM of the robot.

Finally, as the robot is modelled with the possibility of tilt, it is necessary to include the effect that gravity has on the robot. In the $\mathcal{M}$-frame the gravity force $\tilde{F}_g$ is simply

$$\tilde{F}_g = \begin{bmatrix} ma_{gx} \\ ma_{gy} \\ ma_{gz} \end{bmatrix} = R_{\bar{\psi}} \begin{bmatrix} 0 \\ 0 \\ -mg \end{bmatrix} \tag{8}$$

The rotational motion of the robot is generated by the wheel forces F_{xi} and F_{yi}, $i = 1, \ldots, 4$ projected onto the line perpendicular to the line between CoM and the point of contact of wheel i. The angular acceleration around CoM can then be found by multiplying the projected forces by the arms (κ_i), summing over the four wheels and dividing by the moment of inertia.

The total model can thus be seen to be on the form

$$\ddot{\tilde{\chi}} = R_{\bar{\psi}}^{-1} a(\chi, \dot{\chi}, \dot{\phi}, \beta_{ref}, \tau_{ref}) \tag{9}$$

where

$$a = \sum_{i=1}^{4} \begin{bmatrix} \frac{1}{m}\Big(\cos(\beta_i + \theta)\|F_{xi}\| - \sin(\beta_i + \theta)\|F_{yi}\| \Big) - \dot{y}\dot{\theta} - a_{gx} \\ \frac{1}{m}\Big(\sin(\beta_i + \theta)\|F_{xi}\| + cos(\beta_i + \theta)\|F_{yi}\| \Big) + \dot{x}\dot{\theta} - \tilde{a}_{gy} \\ \frac{1}{I}\Big(\sin(\beta_i - \tilde{\gamma}_i)\tilde{\kappa}_i\|F_{xi}\| + \cos(\tilde{\gamma}_i - \beta_i)\kappa_i\|F_{yi}\| \Big) \end{bmatrix}$$

$\|F_{xi}\| = \tau_i / r_w$ represent the propulsion forces and $\tilde{F}_{yi}$ are given by the tire model (3) The moment of inertia I and the wheel radius r_w have been measured to $I = 95 kgm^2$ and $r_w = 0.23m$, respectively.

In Figure 4 a block diagram of the integrated model is shown. From this figure, it is clearly illustrated that the equations of motion described in the $\mathcal{M}$-frame are governed by the wheel orientations and applied torques.

3 Sensor Fusion

The purpose of the sensor fusion is to estimate the state vector of the robot $[\bar{\chi}^T \ \dot{\bar{\chi}}^T] = [\bar{x}, \bar{y}, \bar{\theta}, \dot{x}, \dot{y}, \dot{\theta}]$ using the dynamic model derived above.

When dealing with state estimation in mobile robot applications the prevailing approach is to use a kinematic model for the robot in an Extended Kalman Filter (EKF) [3]. This approach leads to some undesired effects, however, as it removes part of the feedback loop in the filter due to the fact that a kinematic model often calculates the velocities of the robot ($\dot{\bar{\chi}}$) directly from the odometry data obtained from the wheels. This means that only the estimation of χ benefits from the favorable properties of the filter used for the estimation. Another undesirable effect is that part of the EKF approach is to use linearized system and measurement models for calculating the estimate of the mean and covariance of the state vector.

In order to avoid these potential problems, another approach is undertaken here where the robot model (9) is used in an Unscented Kalman Filter (UKF). This is done in order to investigate if the more advanced filter and the model
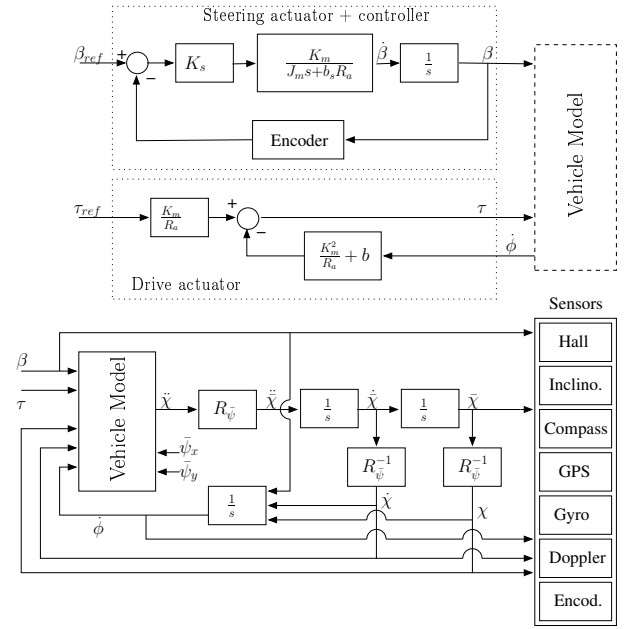

Figure 4. The integrated model complete with actuators, robot model and sensor models.

derived above yield a more accurate estimation compared to an EKF with a standard kinematic model.

The UKF was first proposed in [4] and has later been refined by [7] – it addresses the problem with the first order linearization used in the EKF which can introduce large prediction errors in the estimation process. It is based on the so-called Unscented Transformation, which is used to calculate mean and covariance values for a random variable through a deterministic sampling approach. Define an augmented system state vector $\xi \in \mathbb{R}^2 \times \mathbb{S} \times \mathbb{R}^3 \times \mathbb{R}^6$ by possible non-additive process and measurement noise terms ν as $\xi = [\bar{\chi}^T \ \dot{\bar{\chi}}^T \ \nu^T]$. The Unscented Transformation now propagates this augmented system state using a number of carefully selected sample points $\mathcal{X}_{0,k-1}, \ldots, \mathcal{X}_{2n,k-1}$, where n is the number of states in the augmented state vector, through the non-linear model to evaluate the mean and covariance of the state estimate (refer to the algorithm shown in Table 1).

This approach means that the linearization of the model needed for an EKF – which would have been complicated for the dynamic model due to the discontinuous tire-model – is not needed, and the dynamic model can be used directly in the UKF. The measurement model includes all sensor measurements, except the row camera. Figure 5 shows a block diagram of how the UKF receives measurement signals and calculates the corresponding state estimates.

There is a discontinuity in the compass output θ, as it wraps around at 2π is solved by letting the old estimated state of the angle (in $\hat{\xi}_{k-1}$) wrap when the compass output does, thus keeping them aligned. The different sensors output measurements at different sampling rates and as it is

Predict:

$$\mathcal{X}_{0,k-1} = \hat{\xi}_{k-1}$$

$$\mathcal{X}_{j,k-1} = \hat{\xi}_{k-1} + \left(\sqrt{(n+\kappa_u)P^+_{k-1}}\right)_j, \; j=1,\dots,n$$

$$\mathcal{X}_{j,k-1} = \hat{\xi}_{k-1} - \left(\sqrt{(n+\kappa_u)P^+_{k-1}}\right)_{j-n}, \; j=n+1,\dots,2n$$

$$\mathcal{X}_{k|k-1} = f(\mathcal{X}_{k-1}, u)$$

$$\hat{\xi}^-_k = \sum_{j=0}^{2n} W^m_j \mathcal{X}_{j,k|k-1}$$

$$P^-_k = \sum_{j=0}^{2n} W^c_j (\mathcal{X}_{j,k|k-1} - \hat{\xi}^-_k)(\mathcal{X}_{j,k|k-1} - \hat{\xi}^-_k)^T + Q_k$$

$$\mathcal{Z}_{k|k-1} = h(\mathcal{X}_{k|k-1})$$

$$\hat{z}_k = \sum_{j=0}^{2n} W^m_j \mathcal{Z}_{j,k|k-1}$$

Update:

$$P_{\hat{z}_k \hat{z}_k} = \sum_{j=0}^{2n} W^c_j (\mathcal{Z}_{j,k|k-1} - \hat{z}_k)(\mathcal{Z}_{j,k|k-1} - \hat{z}_k)^T + R_k$$

$$P_{\hat{\xi}^-_k \hat{z}_k} = \sum_{j=0}^{2n} W^c_j (\mathcal{X}_{j,k|k-1} - \hat{\xi}^-_k)(\mathcal{Z}_{j,k|k-1} - \hat{z}_k)^T$$

$$K_k = P_{\hat{x}^-_k \hat{z}_k} P^{-1}_{\hat{z}_k \hat{z}_k}$$

$$\hat{\xi}^+_k = \hat{\xi}^-_k + K_k(z_k - \hat{z}_k)$$

$$P^+_k = P^-_k - K_k P_{\hat{z}_k \hat{z}_k} K^T_k$$

Table 1. UKF algorithm based on the (discrete-time) system model $\xi_k = f(\xi_{k-1}, \nu^\xi_{k-1}, u_{k-1}, z_k = h(\xi_k, \nu^z_{k-1}))$. W_i are weighting factors, P is the covariance estimate and K is the Kalman gain. For further details, see [7].
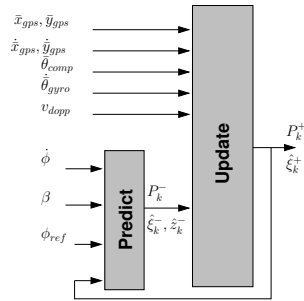

Figure 5. The operation of the UKF.

undesirable to use an old sensor measurement the different sensors are disabled when they do not have new data. This is done by raising the corresponding value in the measurement noise R_k very large and thereby effectively disabling the involved sensor.

4 Simulation and Verification

In Figure 6 the result of a representative verification drive is shown. The simulation data is generated by feeding the recorded control signals from the robot through the dynamic model (9). It is clear that there is good consistency between the measured and the simulated results, especially
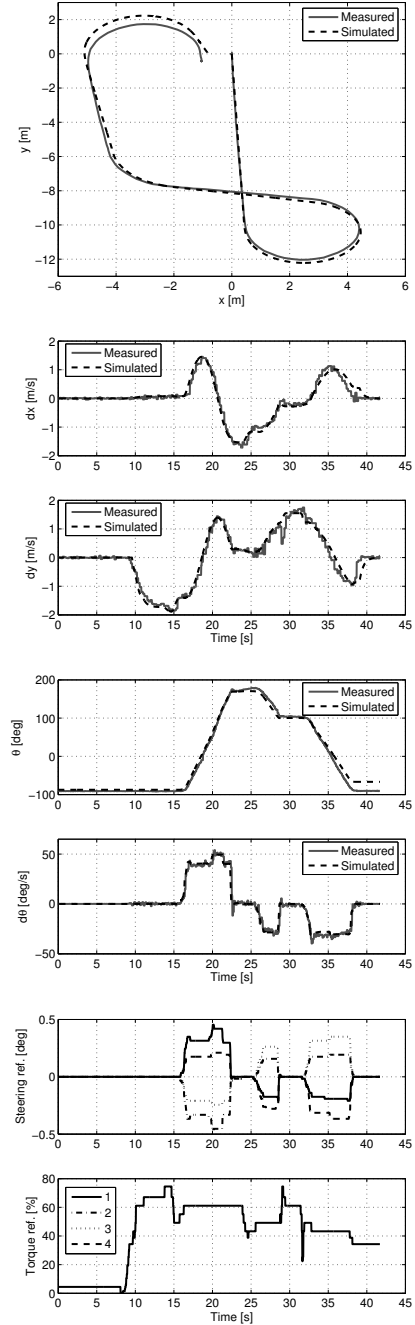
when considering the velocity.

Figure 6. Comparison between simulation and actually driven path. Top to bottom: Path driven by the vehicle; velocity in the $\bar{x}$-direction; velocity in the $\bar{y}$-direction; orientation; rotation. The two bottom figures show the control signals.

In Figure 7 the result from a test of the two sensor fusions is shown and it can be seen that both filters perform satisfactorily in the estimation of the posture (χ). However a clear difference can be seen in the velocity estimates where the UKF exhibits a much lower noise level than the

EKF. The high frequency noise on the EKF estimate originates from noise in the odometry measurements.
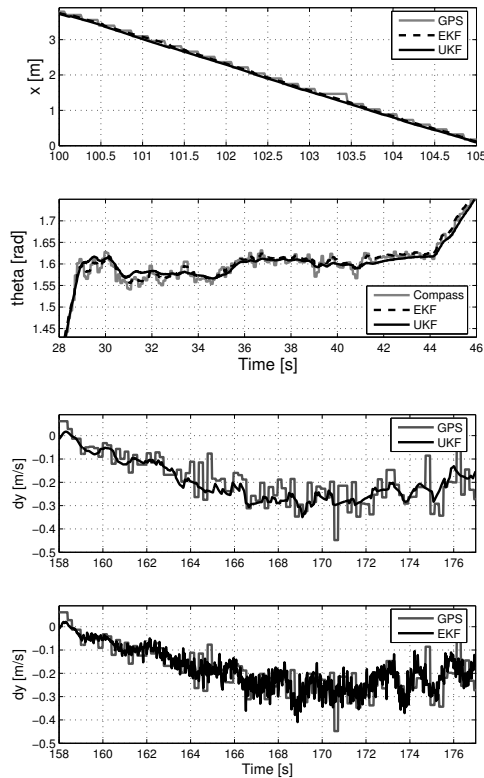

Figure 7. Comparison between sensor measurements, Extended Kalman Filter and Unscented Kalman Filter ($\bar{x}$, θ and $\dot{\bar{y}}$ selected as examples).

5 Conclusion

This paper presented a first-principles model for a four-wheel driven, four-wheel steered mobile robot for autonomous agricultural field surveying. The model takes friction and slip of the wheels into account, and calculates sideways and propulsion forces, which in turn governs the accelerations of the robot body. The model is based on Newtonian mechanics. The purpose of constructing the model was, in addition to obtaining an effective simulation model, to apply it in sensor fusion and (eventually) fault detection and fault-tolerant control. The Unscented Kalman Filter algorithm was then presented, and a practical application of the model and sensor fusion was validated in actual test runs in an outdoor environment.

There is no doubt that both the EKF and the UKF perform satisfactorily and that there in most cases are only little difference on their performance. The major advantage with using the combination of the UKF and the dynamic model compared to the traditional EKF and kinematic model combination is the clear improvement in the velocity estimates. Also the UKF performs somewhat better when operating without the absolute measurements from the GPS.

It can also be concluded that while the UKF have a theoretically better estimation accuracy the practical results show that this advantage is diminished when the filter are executed at a relatively high sampling frequency (in this case 50Hz), since sampling fast reduces the linearization errors. A by far larger source of estimation errors is modelling uncertainties which in this case mainly originates from the wheel skidding and slipping. This is the reason for the better performance of the UKF in this case, as it is based on the tire friction model presented in Section 2.3.

In future research, a natural extension to the UKF would be to incorporate a parameter estimation which continuously estimates the friction of the surface through the cornering stiffness.

References

[1] G. Campion, G. Bastin, and B. D'Andrea-Novel. Structural properties and classification of kinematic and dynamic models of wheeled mobile robots. *IEEE Transactions on Robotics and Automation*, 12, 1996.

[2] B. D'Andrea-Novel, G. Campion, and G. Bastin. Modeling and control of non holonomic wheeled mobile robots. In *Proc. of the 1991 IEEE International Conference on Robotics and Automation*, 1991.

[3] H. R. Everett J. Borenstein and L. Feng. *Navigating Mobile Robots: Sensors and Techniques*. Wellesley, 1999.

[4] Simon J. Julier and Jeffrey K. Uhlmann. *A New Extension of the Kalman Filter to Nonlinear Systems*. University of Oxford, 1997.

[5] Eric J. Rossetter and J. Christian Gerdes. *A Study of Lateral Vehicle Control Under a 'Virtual' Force Framework*. Stanford University, 2002.

[6] K. Thanjavur and R. Rajagopalan. Ease of dynamic modelling of wheled mobile robots using kane's approach. In *Proc. of the 1997 IEEE International Conference on Robotics and Automation*, 1997.

[7] Eric A. Wan and Rudolph van der Merwe. *The Unscented Kalman Filter for Nonlienar Estimation*. Oregon Graduate Institute of Science and Technology, 2000.

[8] Ssu-Hsin Yu and John J. Moskwa. A global approach to vehicle control: Coordination of four wheel steering and wheel torques. *ASME Journal of Dynamical Systems, Measurement and Control*, 116, 1994.